Thermal-Noise Cancellation for Optomechanically Induced Nonreciprocity in a Whispering-Gallery-Mode Microresonator

Zhi-Xiang Tang and Xun-Wei Xu*

Key Laboratory of Low-Dimensional Quantum Structures and Quantum Control of Ministry of Education, Key Laboratory for Matter Microstructure and Function of Hunan Province, Department of Physics and Synergetic Innovation Center for Quantum Effects and Applications, Hunan Normal University, Changsha 410081, China

(Received 19 October 2022; revised 11 January 2023; accepted 10 February 2023; published 28 March 2023)

Magnetic-free optomechanically induced nonreciprocity may stimulate a wide range of practical applications in quantum technologies. However, how to suppress the thermal-noise flow from the mechanical reservoir is still a difficulty encountered in achieving optomechanically nonreciprocal effects on a few- and even single-photon level. Here, we show how to realize thermal-noise cancellation by quantum interference for optomechanically induced nonreciprocity in a whispering-gallery-mode (WGM) microresonator. We find that both nonreciprocal transmission and amplification can be achieved in the WGM microresonator when coupled to two coupled mechanical resonators. More interestingly, the thermal noise can be suppressed when the two coupled mechanical resonators couple to a common thermal reservoir. The thermal-noise cancellation is induced by the destructive quantum interference between the two flow paths of the thermal noises from the common reservoir. The scheme of quantum-interference-induced thermal-noise cancellation can be applied in both sideband-resolved and unresolved regimes, even with strong backscattering taken into account. Our work provides an effective way to achieve nonreciprocal effects on a few- or single-photon level without precooling the mechanical mode to the ground state.

DOI: 10.1103/PhysRevApplied.19.034093

I. INTRODUCTION

Cavity optomechanics that explore the effect induced by the interaction between optical and mechanical resonators has been developed very quickly in the past two decades (for a review, see Ref. [1]), and many different topics have been raised in recent years, such as parity-time-symmetry optomechanics [2–5], topological optomechanical lattices [6–13], and optomechanical-induced nonreciprocity [14–20]. Nonreciprocal devices are indispensable elements in both classical and quantum information processing, for steering signal transmission and reducing backscattering. Different from the conventional nonreciprocal devices that are based on the magneto-optical effect, optomechanical systems provide us a magnetic-free platform to achieve nonreciprocity for potential application in designing nonreciprocal optical devices on chip.

Optomechanical-induced nonreciprocity has made remarkable progress in the past few years. As a typical scheme, optical nonreciprocity was proposed based on optomechanical-induced transparency [21–23] or amplification [23–25] in a whispering-gallery-mode (WGM) resonator with single-direction optical drive [15]. Now, isolators [26,27], directional amplifiers [26,27], and circulators [28,29] have been realized experimentally. In addition, there are many other mechanisms that are proposed theoretically or demonstrated experimentally, such as the intrinsic nonlinearity in an optomechanical system [14,30–32], Brillouin scattering in WGM optomechanical systems [33,34], synthetic magnetism generated by a closed loop of optical and mechanical modes [17,35–53], and edge states in topological optomechanical lattices [8,54].

Realizing single-photon nonreciprocity is one the of the most useful orientations of development in optical nonreciprocity. In order to achieve the nonreciprocal effects on a few- and even single-photon level base on optomechanical interaction, one requirement is the thermal noise generated from the mechanical modes should be equal or less than one. It is obvious that the common way for improving the signal-to-noise ratio by enhancing the magnitude of the signal power [29] is unfit for achieving nonreciprocal effects on a few- and single-photon level. One of the most effective ways to suppress the thermal noise is cooling the mechanical resonator in a cryogenic environment [22] or based on sideband cooling [55,56]. Nevertheless, how to suppress the thermal noise without precooling certainly is an interesting and realistic question.

In this paper, we show how to realize thermal-noise cancellation by quantum interference for optomechanically induced nonreciprocity in a WGM microresonator. We note that there is quantum interference for interacting

*xwxu@hunnu.edu.cn

qubits in contact with a common environment, resulting in coherence and entanglement preserving [57–59]. Here, we investigate optical nonreciprocity in an optomechanical system consisting of a WGM microresonator and two mechanical resonators, and the essential ingredient is the two mechanical resonators coupled to a common environment. We find that when the two mechanical resonators share the same thermal reservoir, the thermal-noise flow through the two mechanical resonators may cancel each other by destructive interference. Our work provides an effective way to achieve nonreciprocal effects on a few- and even single-photon level without precooling the mechanical mode to the ground state. A similar proposal may also be used to realize thermal-noise cancellation for other applications of optomechanics in quantum technologies [60].

The remainder of the paper is organized as follows. In Sec. II, the Hamiltonian of a multimode optomechanical system is introduced, and the spectra of the output fields are obtained formally. The optical nonreciprocal response and thermal-noise cancellation in both sideband-resolved and unresolved regimes are discussed in Sec. III. We summarize this work in Sec. IV.

II. PHYSICAL MODEL

We consider a multimode optomechanical system consisting of a WGM microresonator with two degenerate counterpropagating optical modes (a_L and a_R, frequency ω_c), and two nanomechanical resonators (b_1 and b_2, with degenerate frequency ω_m), as schematically shown in Fig. 1(a). The optical modes (a_L and a_R) are coupled to the mechanical resonator b_1 through their evanescent fields with single-photon optomechanical coupling rate g. Such near-field optomechanical schemes have already been demonstrated by doubly clamped SiN nanostrings or two-dimensional (2D) sheet evanescent coupling to an optical microresonator in experiments [61–63]. The two mechanical resonators are coupled to each other directly via the coupling overhang with strength J_m and indirectly by the phononic crystal [23] (common reservoir R_0) supporting them on both ends. In order to enhance the optomechanical coupling, a strong pumping field (strength Ω, frequency ω_p) is input from the left through a tapered fiber evanescently coupled to the microresonator. The system can be described by a Hamiltonian in the frame rotating at the frequency of the pumping field ω_p as ($\hbar = 1$):

$$\begin{aligned} H_{\rm sys} = & \sum_{k=R,L} \left[\Delta_0 - g\left(b_1^\dagger + b_1\right)\right] a_k^\dagger a_k \\ & + \omega_m \left(b_1^\dagger b_1 + b_2^\dagger b_2\right) + J_m \left(b_1^\dagger + b_1\right)\left(b_2^\dagger + b_2\right) \\ & + J_s \left(a_R^\dagger a_L + a_L^\dagger a_R\right) + \left(\Omega a_R^\dagger + \Omega^* a_R\right), \end{aligned} \tag{1}$$

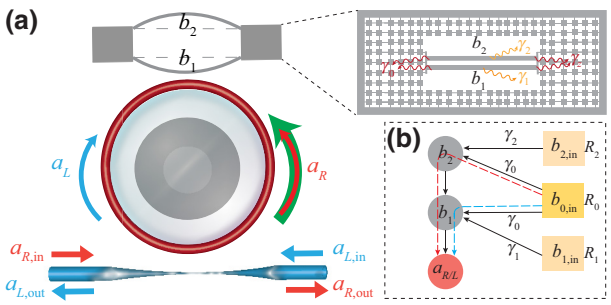

FIG. 1. (a) Schematic diagram of a multimode optomechanical system consisting of a WGM microresonator with two counterpropagating optical modes (a_L and a_R), and two nanomechanical resonators (b_1 and b_2) with degenerate frequency ω_m. The optical modes (a_L and a_R) are coupled to the mechanical resonator b_1 through their evanescent field, and the two nanomechanical resonators (b_1 and b_2) couple with each other directly via the coupling overhang and indirectly by the phononic crystal (common reservoir R_0). (b) Flow chart depicting the thermal-noise ($b_{i,\rm in}$, $i = 0, 1, 2$) flow from the three reservoirs (R_i) to the optical modes $a_{R/L}$. The red and blue dashed curves with an arrowhead depict the two different flow paths from R_0 (common reservoir) to $a_{R/L}$.

where $\Delta_0 = \omega_c - \omega_p$ is the detuning of the cavity mode from the pumping field, and J_s is the coupling strength between the counterpropagating optical modes (a_L and a_R) induced by backscattering.

Before the quantitative calculation, we would like to introduce the physical mechanism that induces the thermal-noise cancellation based on the thermal-noise flow chart [64] as shown in Fig. 1(b). There are three independent thermal reservoirs (R_0, R_1, and R_2), where R_0 denotes the common reservoir for the two mechanical resonators, and R_1 and R_2 denote their respective reservoirs. The common reservoir R_0 can either be a phononic crystal [23,65,66] as shown in Fig. 1(a) or an acoustic waveguide [16,67–70]. γ_0 is the decay rate of the two mechanical resonators to the common reservoir with the input thermal noise $b_{0,\rm in}$. There are two paths for the thermal-noise flow from reservoir R_0 to the optical modes denoting by red and blue dashed curves with an arrowhead in Fig. 1(b). As the thermal noise coming from the same reservoir, the thermal-noise flow through different paths could cancel each other by destructive interference, which is the physical mechanism for the thermal-noise cancellation discussed in this paper. The phononic decays also can be induced by the scattering effect for the surface roughness and material inhomogeneity or the absorption of the material [66], which can be totally described by the coupling of the mechanical resonator b_i to the reservoir R_i with the decay rate γ_i and input thermal noise $b_{i,\rm in}$ ($i = 1, 2$).

Experimentally, the decay rate γ_i as small as $\omega_m/10^{10}$ has been obtained by careful design [66]. The reservoirs R_1 and R_2 are independent of each other, so the thermal-noise flow from them cannot cancel each other by quantum interference. We focus on the case that the phononic decay to the phononic crystal is the dominant process, i.e., $\gamma_0 \gg \gamma_i$, so most of the thermal noise (from the common reservoir R_0) can be cancelled based on quantum interference.

According to the Heisenberg equation of motion and taking into account the damping and corresponding input noise (see Appendix A for details), we get the quantum Langevin equations (QLEs) as

$$\dot{a}_R = -\frac{\kappa}{2}a_R - i\left[\Delta_0 - g\left(b_1^\dagger + b_1\right)\right]a_R - iJ_s a_L - i\Omega + \sqrt{\kappa_{\rm ex}}a_{R,\rm in} + \sqrt{\kappa_0}a_{R,\rm vac}, \tag{2}$$

$$\dot{a}_L = -\frac{\kappa}{2}a_L - i\left[\Delta_0 - g\left(b_1^\dagger + b_1\right)\right]a_L - iJ_s a_R + \sqrt{\kappa_{\rm ex}}a_{L,\rm in} + \sqrt{\kappa_0}a_{L,\rm vac}, \tag{3}$$

$$\dot{b}_1 = -\left(\frac{\gamma_m}{2} + i\omega_m\right)b_1 + ig\left(a_R^\dagger a_R + a_L^\dagger a_L\right) - \frac{\gamma_0}{2}b_2 - iJ_m\left(b_2 + b_2^\dagger\right) + \sqrt{\gamma_0}b_{0,\rm in} + \sqrt{\gamma_{\rm in}}b_{1,\rm in}, \tag{4}$$

$$\dot{b}_2 = -\left(\frac{\gamma_m}{2} + i\omega_m\right)b_2 - iJ_m\left(b_1 + b_1^\dagger\right) - \frac{\gamma_0}{2}b_1 + \sqrt{\gamma_0}b_{0,\rm in} + \sqrt{\gamma_{\rm in}}b_{2,\rm in}. \tag{5}$$

Here $\kappa = \kappa_{\rm ex} + \kappa_0$ is the total decay rate of the optical modes; $\kappa_{\rm ex}$ is external decay rate through the tapered fiber with the input field $a_{k,\rm in}$, and κ_0 is the internal decay rate with the input vacuum noise $a_{k,\rm vac}$; $\gamma_m = \gamma_0 + \gamma_{\rm in}$ is the total decay rate of the two mechanical resonators with $\gamma_{\rm in} = \gamma_1 = \gamma_2$. The input fields (noises) $a_{k,\rm in}$, $a_{k,\rm vac}$, $(k = R, L)$, and $b_{i,\rm in}$ $(i = 0, 1, 2)$ satisfy the correlation relations

$$\left\langle a_{k,\rm in}^\dagger\left(t'\right)a_{k,\rm in}\left(t\right)\right\rangle = S_{k,\rm in}\left(t\right)\delta\left(t + t'\right), \tag{6}$$

$$\left\langle a_{k,\rm vac}^\dagger\left(t'\right)a_{k,\rm vac}\left(t\right)\right\rangle = 0, \tag{7}$$

$$\left\langle b_{i,\rm in}^\dagger\left(t'\right)b_{i,\rm in}\left(t\right)\right\rangle = N_{\rm th}\delta\left(t + t'\right), \tag{8}$$

where $S_{k,\rm in}$ is the spectrum of the input quantum field and $N_{\rm th}$ is the mean numbers of the thermal phonons.

To solve the (nonlinear) QLEs, we can write each operator as the sum of its steady-state value and the quantum noise operator as $a_k = \alpha_k + \delta a_k$ $(k = R, L)$ and $b_i = \beta_i + \delta b_i$ $(i = 1, 2)$. Here the steady-state values α_k and β_i are obtained from the QLEs by using a factorization assumption, e.g., $\langle(b_i^\dagger + b_i)a_k\rangle = (\langle b_i^\dagger\rangle + \langle b_i\rangle)\rangle\langle a_k\rangle$ and $\langle a_k^\dagger a_k\rangle = \langle a_k^\dagger\rangle\langle a_k\rangle$, as

$$\langle a_R\rangle \equiv \alpha_R = \frac{i\Omega}{-\frac{\kappa}{2} - i\omega_m + \frac{J_s^2}{-\frac{\kappa}{2} - i\omega_m}}, \tag{9}$$

$$\langle a_L\rangle \equiv \alpha_L = \frac{iJ_s}{-\frac{\kappa}{2} - i\omega_m}\alpha_R, \tag{10}$$

$$\langle b_1^\dagger\rangle + \langle b_1\rangle = \beta_1^* + \beta_1 = \frac{\Delta_0 - \omega_m}{g}, \tag{11}$$

$$\langle b_2\rangle = \beta_2 \approx -\frac{J_m}{\omega_m}\frac{\Delta_0 - \omega_m}{g}, \tag{12}$$

with setting of $\omega_m = \Delta_0 - g\left(\beta_1^* + \beta_1\right)$. In the strong driving condition $\Omega \gg \kappa$ with $|\langle a_k\rangle|^2 \gg 1$, the dynamic equations for quantum noise operators (δa_k and δb_l) can be linearized by neglecting the nonlinear terms (e.g., $\delta b_i^\dagger \delta a_k$, $\delta b_i \delta a_k$, $\delta a_k^\dagger \delta a_k$), and the linearized QLEs for the quantum noise operators are given by

$$\frac{d}{dt}\delta a_R = \left(-i\omega_m - \frac{\kappa}{2}\right)\delta a_R + iG_R\left(\delta b_1^\dagger + \delta b_1\right) - iJ_s\delta a_L + \sqrt{\kappa_{\rm ex}}a_{R,\rm in} + \sqrt{\kappa_0}a_{R,\rm vac}, \tag{13}$$

$$\frac{d}{dt}\delta a_L = \left(-i\omega_m - \frac{\kappa}{2}\right)\delta a_L + iG_L\left(\delta b_1^\dagger + \delta b_1\right) - iJ_s\delta a_R + \sqrt{\kappa_{\rm ex}}a_{L,\rm in} + \sqrt{\kappa_0}a_{L,\rm vac}, \tag{14}$$

$$\frac{d}{dt}\delta b_1 = \left(-i\omega_m - \frac{\gamma_m}{2}\right)\delta b_1 + iG_R\delta a_R^\dagger + iG_R^*\delta a_R + iG_L^*\delta a_L + iG_L\delta a_L^\dagger - iJ_m\left(\delta b_2 + \delta b_2^\dagger\right) - \frac{\gamma_0}{2}\delta b_2 + \sqrt{\gamma_0}b_{0,\rm in} + \sqrt{\gamma_{\rm in}}b_{1,\rm in}, \tag{15}$$

$$\frac{d}{dt}\delta b_2 = \left(-i\omega_m - \frac{\gamma_m}{2}\right)\delta b_2 - iJ_m\left(\delta b_1^\dagger + \delta b_1\right) - \frac{\gamma_0}{2}\delta b_1 + \sqrt{\gamma_0}b_{0,\rm in} + \sqrt{\gamma_{\rm in}}b_{2,\rm in}, \tag{16}$$

where $G_R \equiv g\alpha_R$ and $G_L \equiv g\alpha_L$ are the effective optomechanical coupling rate.

The linearized QLEs can be concisely expressed as

$$\frac{d}{dt}V\left(t\right) = -MV\left(t\right) + V_{\rm in}\left(t\right), \tag{17}$$

where $V(t)$ is the vector for the quantum noise operators defined by $V(t) \equiv \left(\delta a_R\ \ \delta a_L\ \ \delta b_1\ \ \delta b_2\ \ \delta a_R^\dagger\ \ \delta a_L^\dagger\ \ \delta b_1^\dagger\ \ \delta b_2^\dagger\right)^T$ (superscript T denotes matrix transpose), $V_{\rm in}(t)$ is the input field operator vectors defined by

$$V_{\text{in}}(t) \equiv \begin{pmatrix} \sqrt{\kappa_{\text{ex}}}a_{R,\text{in}} + \sqrt{\kappa_0}a_{R,\text{vac}} \\ \sqrt{\kappa_{\text{ex}}}a_{L,\text{in}} + \sqrt{\kappa_0}a_{L,\text{vac}} \\ \sqrt{\gamma_0}b_{0,\text{in}} + \sqrt{\gamma_{\text{in}}}b_{1,\text{in}} \\ \sqrt{\gamma_0}b_{0,\text{in}} + \sqrt{\gamma_{\text{in}}}b_{2,\text{in}} \\ \sqrt{\kappa_{\text{ex}}}a^{\dagger}_{R,\text{in}} + \sqrt{\kappa_0}a^{\dagger}_{R,\text{vac}} \\ \sqrt{\kappa_{\text{ex}}}a^{\dagger}_{L,\text{in}} + \sqrt{\kappa_0}a^{\dagger}_{L,\text{vac}} \\ \sqrt{\gamma_0}b^{\dagger}_{0,\text{in}} + \sqrt{\gamma_{\text{in}}}b^{\dagger}_{1,\text{in}} \\ \sqrt{\gamma_0}b^{\dagger}_{0,\text{in}} + \sqrt{\gamma_{\text{in}}}b^{\dagger}_{2,\text{in}} \end{pmatrix}, \tag{18}$$

and the coefficient matrix M is given by

$$M = \begin{pmatrix} i\omega_m + \frac{\kappa}{2} & iJ_s & -iG_R & 0 & 0 & 0 & -iG_R & 0 \\ iJ_s & i\omega_m + \frac{\kappa}{2} & -iG_L & 0 & 0 & 0 & -iG_L & 0 \\ -iG_R^* & -iG_L^* & i\omega_m + \frac{\gamma_m}{2} & iJ_m + \frac{\gamma_0}{2} & -iG_R & -iG_L & 0 & iJ_m \\ 0 & 0 & iJ_m + \frac{\gamma_0}{2} & i\omega_m + \frac{\gamma_m}{2} & 0 & 0 & iJ_m & 0 \\ 0 & 0 & iG_R^* & 0 & \frac{\kappa}{2} - i\omega_m & -iJ_s & iG_R^* & 0 \\ 0 & 0 & iG_L^* & 0 & -iJ_s & \frac{\kappa}{2} - i\omega_m & iG_L^* & 0 \\ iG_R^* & iG_L^* & 0 & -iJ_m & iG_R & iG_L & \frac{\gamma_m}{2} - i\omega_m & -iJ_m + \frac{\gamma_0}{2} \\ 0 & 0 & -iJ_m & 0 & 0 & 0 & -iJ_m + \frac{\gamma_0}{2} & \frac{\gamma_m}{2} - i\omega_m \end{pmatrix}. \tag{19}$$

The stability of the system is determined by M, and it is stable only if the real parts of all the eigenvalues of M are positive. In the following discussions, we make sure that the stability conditions are satisfied in all cases.

The linearized QLEs can be solved analytically in the frequency domain with the method of Fourier transform. By introducing the Fourier transform for operator O as

$$O(\omega) = \frac{1}{\sqrt{2\pi}} \int_{-\infty}^{+\infty} O(t) \exp(i\omega t)\, dt, \tag{20}$$

the solution to the linearized QLEs in the frequency domain is obtained as

$$V(\omega) = U(\omega)\, V_{\text{in}}(\omega), \tag{21}$$

where $U(\omega) \equiv (M - i\omega I)^{-1}$, and I denotes the identity matrix. The output fields from the WGM microresonator are obtained based on the input-output relation [71]

$$\delta a_{k,\text{out}} + \delta a_{k,\text{in}} = \sqrt{\kappa_{\text{ex}}}\delta a_k, \qquad (k = R,\ L). \tag{22}$$

By the definition of the input and output spectra

$$S_{k,\text{in}}(\omega) = \int \left\langle \delta a^{\dagger}_{k,\text{in}}(\omega')\, \delta a_{k,\text{in}}(\omega) \right\rangle d\omega', \tag{23}$$

$$S_{k,\text{out}}(\omega) = \int \left\langle \delta a^{\dagger}_{k,\text{out}}(\omega')\, \delta a_{k,\text{out}}(\omega) \right\rangle d\omega', \tag{24}$$

the explicit expressions for the output spectra read

$$\begin{aligned} S_{R,\text{out}}(\omega) &= T_R(\omega)\, S_{R,\text{in}}(\omega) + R_R(\omega)\, S_{L,\text{in}}(\omega) \\ &\quad + S_{R,\text{th}}(\omega) + S_{R,\text{vac}}(\omega), \end{aligned} \tag{25}$$

$$\begin{aligned} S_{L,\text{out}}(\omega) &= T_L(\omega)\, S_{L,\text{in}}(\omega) + R_L(\omega)\, S_{R,\text{in}}(\omega) \\ &\quad + S_{L,\text{th}}(\omega) + S_{L,\text{vac}}(\omega), \end{aligned} \tag{26}$$

with the transmission spectra

$$T_R(\omega) = |\kappa_{\text{ex}} U_{11}(\omega) - 1|^2 + \kappa_{\text{ex}}^2 |U_{15}(\omega)|^2, \tag{27}$$

$$T_L(\omega) = |\kappa_{\text{ex}} U_{22}(\omega) - 1|^2 + \kappa_{\text{ex}}^2 |U_{26}(\omega)|^2, \tag{28}$$

the reflection spectra

$$R_R(\omega) = \kappa_{\text{ex}}^2 |U_{12}(\omega)|^2 + \kappa_{\text{ex}}^2 |U_{16}(\omega)|^2, \tag{29}$$

$$R_L(\omega) = \kappa_{\text{ex}}^2 |U_{21}(\omega)|^2 + \kappa_{\text{ex}}^2 |U_{25}(\omega)|^2, \tag{30}$$

the thermal-noise spectra of mechanical modes

$$S_{R,\mathrm{th}}(\omega) = \kappa_{\mathrm{ex}}\gamma_0\left[|U_{13}(\omega)+U_{14}(\omega)|^2+|U_{17}(\omega)+U_{18}(\omega)|^2\right]N_{\mathrm{th}} + \kappa_{\mathrm{ex}}\gamma_{\mathrm{in}}\left[|U_{13}(\omega)|^2+|U_{14}(\omega)|^2+|U_{17}(\omega)|^2+|U_{18}(\omega)|^2\right]N_{\mathrm{th}}, \tag{31}$$

$$S_{L,\mathrm{th}}(\omega) = \kappa_{\mathrm{ex}}\gamma_0\left[|U_{23}(\omega)+U_{24}(\omega)|^2+|U_{27}(\omega)+U_{28}(\omega)|^2\right]N_{\mathrm{th}} + \kappa_{\mathrm{ex}}\gamma_{\mathrm{in}}\left[|U_{23}(\omega)|^2+|U_{24}(\omega)|^2+|U_{27}(\omega)|^2+|U_{28}(\omega)|^2\right]N_{\mathrm{th}}, \tag{32}$$

and the vacuum quantum noise spectra,

$$S_{R,\mathrm{vac}}(\omega) = \kappa_{\mathrm{ex}}^2|U_{15}(\omega)|^2+\kappa_{\mathrm{ex}}\kappa_0|U_{15}(\omega)|^2+\kappa_{\mathrm{ex}}^2|U_{16}(\omega)|^2+\kappa_{\mathrm{ex}}\kappa_0|U_{16}(\omega)|^2 + \kappa_{\mathrm{ex}}\gamma_0|U_{17}(\omega)+U_{18}(\omega)|^2+\kappa_{\mathrm{ex}}\gamma_{\mathrm{in}}\left[|U_{17}(\omega)|^2+|U_{18}(\omega)|^2\right], \tag{33}$$

$$S_{L,\mathrm{vac}}(\omega) = \kappa_{\mathrm{ex}}^2|U_{25}(\omega)|^2+\kappa_{\mathrm{ex}}\kappa_0|U_{25}(\omega)|^2+\kappa_{\mathrm{ex}}^2|U_{26}(\omega)|^2+\kappa_{\mathrm{ex}}\kappa_0|U_{26}(\omega)|^2 + \kappa_{\mathrm{ex}}\gamma_0|U_{27}(\omega)+U_{28}(\omega)|^2+\kappa_{\mathrm{ex}}\gamma_{\mathrm{in}}\left[|U_{27}(\omega)|^2+|U_{28}(\omega)|^2\right]. \tag{34}$$

Here, $U_{nm}(\omega)$ (for $n,m=1,\ldots,8$) represents the element at the nth row and mth column of the matrix $U(\omega)$.

III. RESULTS AND DISCUSSIONS

In this section, we study the optical nonreciprocal response in both sideband-resolved and unresolved regimes. In order to show the effect of thermal-noise cancellation, we compare the thermal-noise spectra for a WGM microresonator coupling to two coupled mechanical resonators with the case of the WGM microresonator coupling to only one mechanical resonator. Moreover, we discuss the effects of backscattering in the WGM microresonator on the optical nonreciprocal response and thermal-noise cancellation before the end of this section.

A. Nonreciprocal transmission in the sideband-resolved regime

In this subsection, we assume that the system is working in the sideband-resolved regime with mechanical frequency $\omega_m > \kappa_0$, which is within the reach of recent experiments. As reported in Ref. [61], the doubly clamped SiN nanostrings with fundamental resonance frequencies $\Omega_m/2\pi = 6.5-16$ MHz and mechanical quality factors of $Q_m = 10^4-10^5$ are coupled to the optical modes of toroid silica microcavity (unloaded optical linewidth of 4.9 MHz) through evanescent field. Furthermore, the mechanical resonators with high frequency ranging from 100 MHz to a few GHz have been realized in the mechanical devices with smaller size or greater stiffness [72–75].

For comparison, we consider a WGM microresonator coupling to one nanomechanical resonator (denoted by b_1) first, with the schematic diagram of b_1 shown in Fig. 2(a). b_1 couples to reservoir R_0 (i.e., the phononic crystal) for phonon loss from the both ends (γ_0), and to the reservoir R_1 for the surface roughness and material inhomogeneity or the absorption of the material (γ_1), simultaneously. This model can be described by the total Hamiltonian (A1) in Appendix A with all the parameters related to b_2 setting to zero. The corresponding transmission spectra $T_R(\omega)$ and $T_L(\omega)$, and the thermal-noise spectrum $S_{R,\mathrm{th}}(\omega)/N_{\mathrm{th}}$ are shown in Figs. 2(b) and 2(c). As predicted theoretically in Ref. [15] and experimentally demonstrated

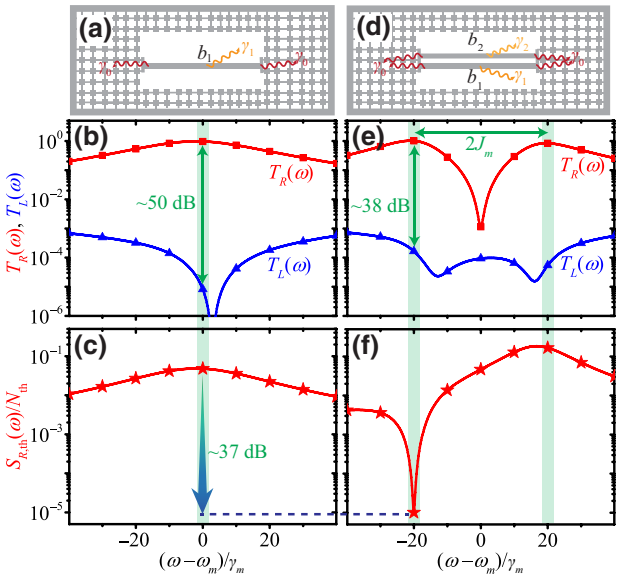

FIG. 2. Schematic diagrams of (a) one nanomechanical resonator and (d) two coupled nanomechanical resonators. (b) The transmission spectra $T_R(\omega)$ and $T_L(\omega)$, and (c) the thermal-noise spectrum $S_{R,\mathrm{th}}(\omega)/N_{\mathrm{th}}$ for the WGM microresonator coupling to one mechanical resonator, (e) $T_R(\omega)$ and $T_L(\omega)$, and (f) $S_{R,\mathrm{th}}(\omega)/N_{\mathrm{th}}$ for the WGM microresonator coupling to two coupled mechanical resonators, in the sideband-resolved regime ($\omega_m = 5\kappa_0$). The other parameters are $\Delta=\omega_m$, $G_R = 0.1\kappa_0$, and $J_m = 0.01\kappa_0$, $J_s = 0.1\kappa_0$, $\kappa_{\mathrm{ex}} = \kappa_0$, $G_L = iJ_sG_R/(-\kappa/2-i\omega_m)$, $\gamma_0 = \omega_m/10^4$, and $\gamma_1=\gamma_2=\omega_m/10^8$.

in Refs. [26–29], an optical isolator with the isolation $I_{R/L} \equiv T_R(\omega)/T_L(\omega)$ as high as 50 dB can be achieved at the resonant frequency $\omega = \omega_m$. However, to achieve the nonreciprocal effects on a few- and even single-photon level, the thermal noise should be considered simultaneously. From Fig. 2(b), we get the thermal-noise spectrum $S_{R,\mathrm{th}}(\omega)/N_{\mathrm{th}} = 0.048$ for the optical isolator working at the frequency $\omega = \omega_m$. According to the Bose-Einstein statistics, the mean numbers of the thermal phonons is given by $N_{\mathrm{th}} = [\exp(\hbar\omega_m/k_B T) - 1]^{-1}$, where k_B is the Boltzmann constant, and T is the temperature of the reservoir at the thermal equilibrium. For example, a mechanical resonator with frequency $\omega_m = 60$ MHz at the room temperature $T = 300$ K, contains about $N_{\mathrm{th}} \approx 10^5$ thermal phonons, then we get the thermal-noise spectrum $S_{R,\mathrm{th}}(\omega) \approx 4800$. In order to improve the signal-to-noise ratio, we need to enhance the magnitude of the signal power [29], or suppress the thermal noise by cooling the mechanical resonator in a cryogenic environment [22] or based on sideband cooling [55,56].

Here, we show that the thermal noise can be suppressed based on quantum interference for the WGM microresonator coupling to two coupled mechanical resonators [Fig. 2(d)], with the transmission spectra $T_R(\omega)$ and $T_L(\omega)$, and thermal-noise spectrum $S_{R,\mathrm{th}}(\omega)/N_{\mathrm{th}}$ shown in Figs. 2(e) and 2(f). Different from the nonreciprocity in the WGM microresonator coupling to one mechanical mode with one transmission window at $\omega = \omega_m$ [15,26–29], there are two peaks around frequencies $\omega_m \pm J_m$ in the transmission spectrum of $T_R(\omega)$ for fields from left to right [see Fig. 2(e)]. At the same time, there are two dips in the transmission spectrum of $T_L(\omega)$ for fields from right to left with the optomechanical interaction G_L enhanced by the backscattering J_s. The optical nonreciprocity with an isolation about 38 dB is achieved at $\omega = \omega_m \pm J_m$ with backscattering effect $J_s = 0.1\kappa_0$ taken into account. Of note, there is a dip in the thermal-noise spectrum $S_{R,\mathrm{th}}(\omega)/N_{\mathrm{th}}$ at the frequency $\omega = \omega_m - J_m$, which is about 37 dB lower than the case for the WGM microresonator coupling to one mechanical resonator [see Figs. 2(c) and 2(f)]. In this case, the thermal-noise spectrum for a mechanical resonator with frequency $\omega_m = 60$ MHz at the room temperature $T = 300$ K is suppressed to $S_{R,\mathrm{th}}(\omega) \approx 1$, which means that we can achieve nonreciprocal transmission with signal-to-noise ratio $s/n \approx 1$ around $\omega = \omega_m - J_m$ on a single-photon level without precooling the mechanical mode to the ground state.

Physically, the thermal-noise suppression (enhancement) is induced by the quantum interference between the two flow paths of the thermal noises from the common reservoir R_0 to the optical modes $a_{R/L}$, as shown by the flow chart in Fig. 1(b). Here, the thermal-noise flow from the common reservoir R_0 to the optical modes $a_{R/L}$ through the mechanical resonator b_1 [blue dashed curves with an arrowhead in Fig. 1(b)] is given by

$$S^{(1)}_{R,\mathrm{th}}(\omega) = \kappa_{\mathrm{ex}}\gamma_m\left[|U_{13}(\omega)|^2 + |U_{17}(\omega)|^2\right]N_{\mathrm{th}}, \quad (35)$$

and the thermal-noise flow through the mechanical resonator b_2 [red dashed curves with an arrowhead Fig. 1(b)] is given by

$$S^{(2)}_{R,\mathrm{th}}(\omega) = \kappa_{\mathrm{ex}}\gamma_m\left[|U_{14}(\omega)|^2 + |U_{18}(\omega)|^2\right]N_{\mathrm{th}}. \quad (36)$$

To reveal the quantum interference more quantitatively, we show the thermal-noise flow for different paths in Fig. 3(a). The strength of the thermal-noise flow by different paths $S^{(1)}_{R,\mathrm{th}}(\omega)$ and $S^{(2)}_{R,\mathrm{th}}(\omega)$ are almost the same value around the frequency $\omega = \omega_m - J_m$, which is one of the critical points for achieving high visibility in destructive interference. The dip in the thermal-noise spectrum at $\omega = \omega_m - J_m$ is induced by the destructive interference with $S^{(1)}_{R,\mathrm{th}}(\omega) \simeq S^{(2)}_{R,\mathrm{th}}(\omega)$.

The thermal-noise suppression can also be understood by introducing the bright and dark modes [76–80] (normal modes) $b_\pm \equiv (b_1 \pm b_2)/\sqrt{2}$. Based on some analytical derivations and Table I in Appendix B, we find that the dark mode b_- with eigenvalue $\omega_m - J_m$ is decoupled from the common reservoir R_0. Meanwhile, the bright mode b_+ with eigenvalue $\omega_m + J_m$ is coupled to the common reservoir R_0 with the strength enhanced by a factor of $\sqrt{2}$. The thermal-noise spectra $S^{(+)}_{R,\mathrm{th}}(\omega)$ and $S^{(-)}_{R,\mathrm{th}}(\omega)$ coming from the bright and dark modes are shown in Fig. 3(b). Clearly, the thermal noise $S^{(-)}_{R,\mathrm{th}}(\omega)$ from the dark mode is

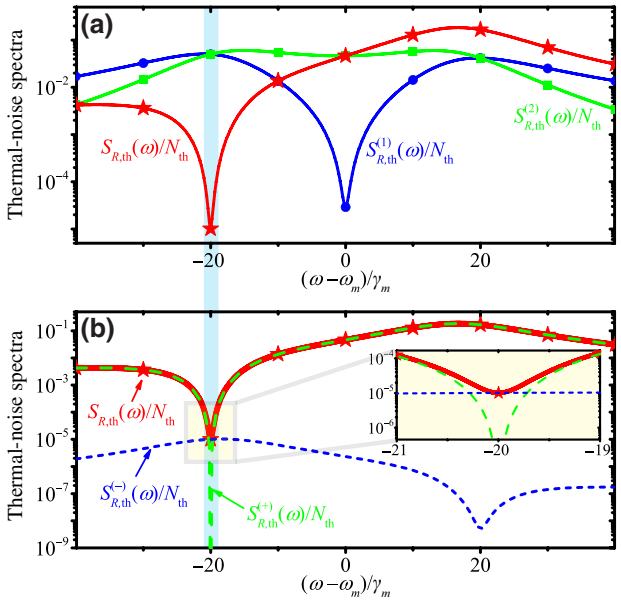

FIG. 3. (a) Thermal-noise spectra $S^{(1)}_{R,\mathrm{th}}(\omega)/N_{\mathrm{th}}$, $S^{(2)}_{R,\mathrm{th}}(\omega)/N_{\mathrm{th}}$, and $S_{R,\mathrm{th}}(\omega)/N_{\mathrm{th}}$, (b) $S^{(+)}_{R,\mathrm{th}}(\omega)/N_{\mathrm{th}}$, $S^{(-)}_{R,\mathrm{th}}(\omega)/N_{\mathrm{th}}$, and $S_{R,\mathrm{th}}(\omega)/N_{\mathrm{th}}$, are plotted as functions of the normalized detuning $(\omega - \omega_m)/\gamma_m$. The other parameters are the same as those given in Fig. 2(d).

much lower than the thermal noise $S^{(+)}_{R,\mathrm{th}}(\omega)$ from the bright mode, except that the $S^{(+)}_{R,\mathrm{th}}(\omega)$ it is dramatically suppressed by quantum interference around the frequency $\omega_m - J_m$ for the dark and bright modes $b_\pm$ coupling to the reservoirs R_1 and R_2 simultaneously [see the inset of Fig. 3(b) and Table I].

B. Nonreciprocal amplification in the sideband-unresolved regime

In this subsection, we discuss the optical nonreciprocal response of the system in the sideband-unresolved regime with mechanical frequency $\omega_m < \kappa_0$, which is also a common situation in recent experiments [62,81,82]. Different from the case in the sideband-resolved regime, the blue sideband transitions play a significant role in the sideband-unresolved regime, which may induce significantly different results in the transmission spectrum.

The transmission spectra in the sideband-unresolved regime are shown in Figs. 4(a) and 4(c). Similarly, there is one peak in the transmission spectrum $T_R(\omega)$ around the frequency ω_m for the WGM microresonator coupling to one mechanical resonator, and two peaks in the transmission spectrum $T_R(\omega)$ around the frequencies $\omega_m \pm J_m$ for the WGM microresonator coupling to two coupled mechanical resonators. The optical nonreciprocity with a isolation about 48 dB is achieved for both of these systems. Moreover, the values of the peaks in $T_R(\omega)$ are greater than one, i.e., nonreciprocal amplification is achieved in sideband-unresolved regime. Different from the amplification achieving with blue-detuned external driving [23–25], here the nonreciprocal amplification is achieved with a red-detuned external driving field in the sideband-unresolved regime.

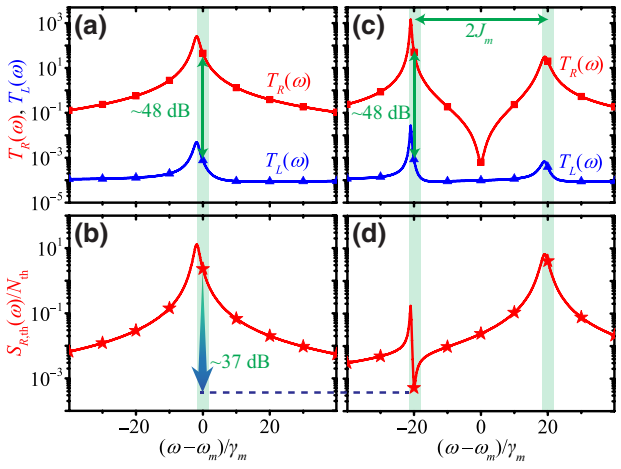

FIG. 4. (a) Transmission spectra $T_R(\omega)$ and $T_L(\omega)$, and (b) the thermal-noise spectrum $S_{R,\mathrm{th}}(\omega)/N_{\mathrm{th}}$ for the WGM microresonator coupling to one mechanical resonator, (c) $T_R(\omega)$ and $T_L(\omega)$, and (d) $S_{R,\mathrm{th}}(\omega)/N_{\mathrm{th}}$ for the WGM microresonator coupling to two coupled mechanical resonators, in the sideband-unresolved regime ($\omega_m = 0.1\kappa_0$). The other parameters are $\Delta = \omega_m$, $G_R = 0.01\kappa_0$, and $J_m = 0.0002\kappa_0$, $J_s = 0.1\kappa_0$, $\kappa_{\mathrm{ex}} = \kappa_0$, $G_L = iJ_sG_R/(-\kappa/2 - i\omega_m)$, $\gamma_0 = \omega_m/10^4$, and $\gamma_1 = \gamma_2 = \omega_m/10^8$.

Physically, nonreciprocal amplification appearing in the sideband-unresolved regime is induced by the blue-sideband transitions. There are both red-sideband transitions for the terms $iG_R\delta b_1$ in Eq. (13) and $iG^*_R\delta a_R$ in Eq. (15), and blue-sideband transitions for the terms $iG_R\delta b^\dagger_1$ in Eq. (13) and $iG_R\delta a^\dagger_R$ in Eq. (15). According to the quantum theory for sideband cooling in optomechanical systems [55,56], the red-sideband transitions correspond to the excitation changing between the optical and mechanical modes, and blue-sideband transitions correspond to the excitation of both optical and mechanical modes simultaneously. The theoretical analysis and experimental results show that the blue-sideband transitions can induced signal absorption and amplification [23–25]. In the sideband-resolved regime, the blue-sideband transitions are suppressed for large detuning. However, in the sideband-unresolved regime, the blue-sideband transitions become significant even with a red-detuned external driving field as discussed here.

The blue-sideband transitions can amplify not only the signal field but also the input thermal noises, which is the origin of optical-induced heating in optomechanical systems [83,84]. As shown in Fig. 4(b), there is a peak in the thermal-noise spectrum around $\omega = \omega_m$ for the WGM microresonator coupling to one mechanical resonator. In contrast, the thermal noise around the frequency $\omega = \omega_m - J_m$ is suppressed dramatically by quantum interference for the WGM microresonator coupling to two coupled mechanical resonators, which is about 37 dB lower than the case for the WGM microresonator coupling to one mechanical resonator [see Fig. 4(d)]. This suggests that the scheme of thermal-noise cancellation for two mechanical resonators coupled to a common environment also works in the sideband-unresolved regimes for nonreciprocal amplification.

C. Effects of backscattering

Before the end of this section, let us discuss the effect of backscattering J_s between the two degenerate counterpropagating optical modes (a_L and a_R) on the optical nonreciprocal response and thermal-noise cancellation in both sideband-resolved and unresolved regimes. In the preceding discussions, the weak backscattering with $J_s = 0.1\kappa_0$ is considered, and nonreciprocal effects are obvious for $|G_R| \gg |G_L|$.

When the backscattering strength J_s becomes larger, the backscattering may strongly redistributes the signal field. In the sideband-resolved regime, the nonreciprocal effect with isolation $I_{R/L} \approx 11$ dB is obtained as shown in

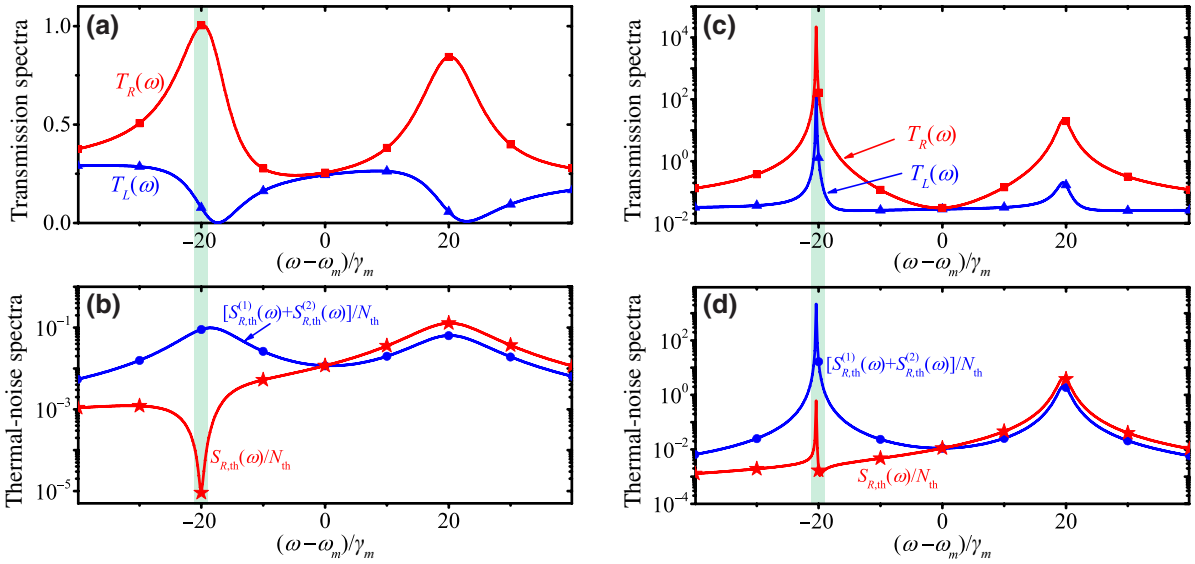

FIG. 5. (a) Transmission spectra $T_R(\omega)$ and $T_L(\omega)$, and (b) the thermal-noise spectra $S_{R,\mathrm{th}}(\omega)/N_{\mathrm{th}}$ and $[S^{(1)}_{R,\mathrm{th}}(\omega)+S^{(2)}_{R,\mathrm{th}}(\omega)]/N_{\mathrm{th}}$ are plotted as functions of the normalized detuning $(\omega-\omega_m)/\gamma_m$ for $\Delta=\omega_m=5\kappa_0$, $J_s=\kappa_0$, $G_R=0.1\kappa_0$, and $J_m=0.01\kappa_0$. (c) $T_R(\omega)$ and $T_L(\omega)$, and (d) $S_{R,\mathrm{th}}(\omega)/N_{\mathrm{th}}$ and $[S^{(1)}_{R,\mathrm{th}}(\omega)+S^{(2)}_{R,\mathrm{th}}(\omega)]/N_{\mathrm{th}}$ are plotted as functions of the normalized detuning $(\omega-\omega_m)/\gamma_m$ for $\Delta=\omega_m=0.1\kappa_0, J_s=0.45\kappa_0$, $G_R=0.01\kappa_0$, and $J_m=0.0002\kappa_0$. The other parameters are $G_L=iJ_sG_R/(-\kappa/2-i\omega_m)$, $\kappa_{\mathrm{ex}}=\kappa_0$, $\gamma_0=\omega_m/10^4$, and $\gamma_1=\gamma_2=\omega_m/10^8$.

Fig. 5(a), where the condition of $|G_R|\gg|G_L|$ is still satisfied for $J_s=\kappa_0$. In contrast, we have $|G_R|\sim|G_L|$ for $J_s=\kappa_0$ in the sideband-unresolved regime, and the system becomes unstable for the negative real parts of the eigenvalues of M in Eq. (19). To guarantee the stability of the system in the sideband-unresolved regime, we take the backscattering strength $J_s=0.45\kappa_0$ as an example, and the transmission spectra with isolation $I_{R/L}\approx 21$ dB is shown in Fig. 5(c).

The scheme of thermal-noise suppression for the two mechanical resonators couple to a common reservoir still works in the strong backscattering condition. In Figs. 5(b) and 5(d), the thermal-noise spectra are shown in both the sideband-resolved and unresolved regimes. By comparison with results of $[S^{(1)}_{R,\mathrm{th}}(\omega)+S^{(2)}_{R,\mathrm{th}}(\omega)]/N_{\mathrm{th}}$, the thermal noise $S_{R,\mathrm{th}}(\omega)/N_{\mathrm{th}}$ around the frequency $\omega=\omega_m-J_m$ is dramatically suppressed in both the sideband-resolved and unresolved regimes. These results indicate that the scheme of quantum-interference-induced thermal noise cancellation is a robust method against backscattering.

IV. CONCLUSIONS

In summary, we propose a scheme to realize thermal-noise cancellation for optomechanically induced nonreciprocity in a WGM microresonator by coupling two mechanical resonators to a common reservoir. We find that nonreciprocal transmission and amplification with high isolation can be achieved in the WGM microresonator for an optomechanical system working in the sideband-resolved and unresolved regimes. More interestingly, the thermal noise can be cancelled by the destructive quantum interference between the two flow paths of the thermal noises from the common reservoir to the optical modes. Numerical results indicate that the scheme of quantum-interference-induced thermal noise cancellation can be applied in both sideband-resolved and unresolved regimes, even with strong backscattering taken into account. Optomechanically induced nonreciprocity with thermal-noise cancellation may stimulate a wide range of practical applications of optomechanical devices in chiral quantum networks [85] and chiral quantum optics [86].

The scheme of quantum-interference-induced thermal-noise cancellation is a general method for thermal-noise suppression in optomechanics with wide applications in quantum technologies [60]. It can be applied to suppress the thermal noise in the microwave-to-optical conversion for optomechanical transducers [87–93]. Similar schemes can also be applied to suppress the thermal noise in quantum sensing via optomechanical interactions [94–96].

ACKNOWLEDGMENTS

This work is by the National Natural Science Foundation of China (Grants No. 12064010 and No. 12247105), Natural Science Foundation of Hunan Province of China (Grant No. 2021JJ20036), and the Science and Technology Innovation Program of Hunan Province (Grant No. 2022RC1203).

APPENDIX A: DERIVATION OF THE QUANTUM LANGEVIN EQUATIONS

The total Hamiltonian of the WGM optomechanical system coupling with the reservoirs is described by

$$H_{\rm tot} = H_{\rm sys} + H_{\rm re} + H_{\rm int}, \tag{A1}$$

where $H_{\rm sys}$ is the optomechanical Hamiltonian Eq. (1) in the main text, $H_{\rm re}$ is the free Hamiltonian of the optical and mechanical reservoirs,

$$H_{\rm re} = \sum_{k=R,L}\int_0^{+\infty} d\omega\omega\left(a^{\dagger}_{k,0,\omega}a_{k,0,\omega} + a^{\dagger}_{k,{\rm ex},\omega}a_{k,{\rm ex},\omega}\right) + \sum_{i=0,1,2}\int_0^{+\infty} d\omega\omega b^{\dagger}_{i,\omega}b_{i,\omega}, \tag{A2}$$

and $H_{\rm int}$ describes the interaction between the reservoirs and the optomechanical system,

$$\begin{aligned} H_{\rm int} = {} & i\sum_{k=R,L}\int_0^{+\infty} d\omega h_{k,{\rm ex}}(\omega)\left[a^{\dagger}_{k,{\rm ex},\omega}a_k - a^{\dagger}_k a_{k,{\rm ex},\omega}\right] \\ & + i\sum_{k=R,L}\int_0^{+\infty} d\omega h_{k,0}(\omega)\left[a^{\dagger}_{k,0,\omega}a_k - a^{\dagger}_k a_{k,0,\omega}\right] \\ & + i\sum_{i=1,2}\int_0^{+\infty} d\omega g_{i,{\rm in}}(\omega)\left[b^{\dagger}_{i,\omega}b_i - b^{\dagger}_i b_{i,\omega}\right] \\ & + i\sum_{i=1,2}\int_0^{+\infty} d\omega g_{i,0}(\omega)\left[b^{\dagger}_{0,\omega}b_i - b^{\dagger}_i b_{0,\omega}\right] \end{aligned} \tag{A3}$$

with the coupling strengths $h_{k,{\rm ex}}(\omega)$, $h_{k,0}(\omega)$, $g_{i,{\rm in}}(\omega)$, and $g_{i,0}(\omega)$. Here, $a_{k,{\rm ex},\omega}$, $a_{k,0,\omega}$, and $b_{i,\omega}$ are the boson annihilation operators for the reservoirs with $\left[a_{k,{\rm ex},\omega}, a^{\dagger}_{k,{\rm ex},\omega'}\right] = \delta\left(\omega-\omega'\right)$, $\left[a_{k,0,\omega}, a^{\dagger}_{k,0,\omega'}\right] = \delta\left(\omega-\omega'\right)$, and $\left[b_{i,\omega}, b^{\dagger}_{i,\omega'}\right] = \delta\left(\omega-\omega'\right)$.

The Heisenberg equations for the operators a_k, b_i, $a_{k,0,\omega}$, $a_{k,{\rm ex},\omega}$, $b_{0,\omega}$, and $b_{i,\omega}$ read

$$\begin{aligned} \frac{da_R}{dt} = {} & -i\left[\Delta_0 - g\left(b^{\dagger}_1 + b_1\right)\right]a_R - iJ_s a_L - i\Omega \\ & - \int_0^{+\infty} d\omega h_{R,{\rm ex}}(\omega)\, a_{R,{\rm ex},\omega} \\ & - \int_0^{+\infty} d\omega h_{R,0}(\omega)\, a_{R,0,\omega}, \end{aligned} \tag{A4}$$

$$\begin{aligned} \frac{da_L}{dt} = {} & -i\left[\Delta_0 - g\left(b^{\dagger}_1 + b_1\right)\right]a_L - iJ_s a_R \\ & - \int_0^{+\infty} d\omega h_{L,{\rm ex}}(\omega)\, a_{L,{\rm ex},\omega} \\ & - \int_0^{+\infty} d\omega h_{L,0}(\omega)\, a_{L,0,\omega}, \end{aligned} \tag{A5}$$

$$\begin{aligned} \frac{db_1}{dt} = {} & -i\omega_m b_1 + ig\sum_{k=R,L} a^{\dagger}_k a_k - iJ_m\left(b^{\dagger}_2 + b_2\right) \\ & - \int_0^{+\infty} d\omega g_{1,{\rm in}}(\omega)\, b_{1,\omega} \\ & - \int_0^{+\infty} d\omega g_{1,0}(\omega)\, b_{0,\omega}, \end{aligned} \tag{A6}$$

$$\begin{aligned} \frac{db_2}{dt} = {} & -i\omega_m b_2 - iJ_m\left(b^{\dagger}_1 + b_1\right) \\ & - \int_0^{+\infty} d\omega g_{2,{\rm in}}(\omega)\, b_{2,\omega} \\ & - \int_0^{+\infty} d\omega g_{2,0}(\omega)\, b_{0,\omega}, \end{aligned} \tag{A7}$$

$$\frac{da_{k,0,\omega}}{dt} = -i\omega a_{k,0,\omega} + h_{k,0}(\omega)\, a_k, \tag{A8}$$

$$\frac{da_{k,{\rm ex},\omega}}{dt} = -i\omega a_{k,{\rm ex},\omega} + h_{k,{\rm ex}}(\omega)\, a_k, \tag{A9}$$

$$\frac{db_{0,\omega}}{dt} = -i\omega b_{0,\omega} + \sum_{i=1,2} g_{i,0}(\omega)\, b_i, \tag{A10}$$

$$\frac{db_{i,\omega}}{dt} = -i\omega b_{i,\omega} + g_{i,{\rm in}}(\omega)\, b_i. \tag{A11}$$

Equations (A8)–(A11) can be solved analytically as

$$a_{k,0,\omega} = a_{k,0,\omega}(t_0)\, e^{-i\omega(t-t_0)} + h_{k,0}(\omega)\int_{t_0}^{t} a_k\left(t'\right) e^{-i\omega\left(t-t'\right)} dt', \tag{A12}$$

$$a_{k,{\rm ex},\omega} = a_{k,{\rm ex},\omega}(t_0)\, e^{-i\omega(t-t_0)} + h_{k,{\rm ex}}(\omega)\int_{t_0}^{t} a_k\left(t'\right) e^{-i\omega\left(t-t'\right)} dt', \tag{A13}$$

$$b_{0,\omega} = b_{0,\omega}(t_0)\, e^{i\omega(t_0-t)} + \sum_{i=1,2}\int_{t_0}^{t} g_{i,0}(\omega)\, b_i\left(t'\right) e^{i\omega\left(t'-t\right)} dt', \tag{A14}$$

$$b_{i,\omega} = b_{i,\omega}(t_0)\, e^{i\omega(t_0-t)} + \int_{t_0}^{t} g_{i,{\rm in}}(\omega)\, b_i\left(t'\right) e^{i\omega\left(t'-t\right)} dt'. \tag{A15}$$

Substitute these solutions into Eqs. (A4)–(A7), we get

$$\frac{da_R}{dt} = -i\left[\Delta_0 - g\left(b_1^\dagger + b_1\right)\right]a_R - iJ_s a_L - i\Omega - \frac{\kappa_{R,\mathrm{ex}} + \kappa_{R,0}}{2}a_R + \sqrt{\kappa_{R,\mathrm{ex}}}a_{R,\mathrm{in}} + \sqrt{\kappa_{R,0}}a_{R,\mathrm{vac}}, \tag{A16}$$

$$\frac{da_L}{dt} = -i\left[\Delta_0 - g\left(b_1^\dagger + b_1\right)\right]a_L - iJ_s a_R - \frac{\kappa_{L,\mathrm{ex}} + \kappa_{L,0}}{2}a_L + \sqrt{\kappa_{L,\mathrm{ex}}}a_{L,\mathrm{in}} + \sqrt{\kappa_{L,0}}a_{L,\mathrm{vac}}, \tag{A17}$$

$$\frac{db_1}{dt} = -i\omega_m b_1 + ig\sum_{k=R,L} a_k^\dagger a_k - iJ_m\left(b_2^\dagger + b_2\right) - \frac{\sqrt{\gamma_{1,0}\gamma_{2,0}}}{2}b_2 - \frac{\gamma_{1,0} + \gamma_{1,\mathrm{in}}}{2}b_1 + \sqrt{\gamma_{1,\mathrm{in}}}b_{1,\mathrm{in}} + \sqrt{\gamma_{1,0}}b_{0,\mathrm{in}}, \tag{A18}$$

$$\frac{db_2}{dt} = -i\omega_m b_2 - iJ_m\left(b_1^\dagger + b_1\right) - \frac{\sqrt{\gamma_{1,0}\gamma_{2,0}}}{2}b_1 - \frac{\gamma_{2,0} + \gamma_{2,\mathrm{in}}}{2}b_2 + \sqrt{\gamma_{2,\mathrm{in}}}b_{2,\mathrm{in}} + \sqrt{\gamma_{2,0}}b_{0,\mathrm{in}}, \tag{A19}$$

based on the Markov approximation $h_{k,\mathrm{ex}}(\omega) = \sqrt{\kappa_{k,\mathrm{ex}}/2\pi}$, $h_{k,0}(\omega) = \sqrt{\kappa_{k,0}/2\pi}$, $g_{i,\mathrm{in}}(\omega) = \sqrt{\gamma_{i,\mathrm{in}}/2\pi}$, $g_{i,0}(\omega) = \sqrt{\gamma_{i,0}/2\pi}$, and the input noise operators are defined by

$$a_{k,\mathrm{in}} \equiv -\frac{1}{\sqrt{2\pi}}\int_0^{+\infty} d\omega a_{k,\mathrm{ex},\omega}(t_0)\, e^{-i\omega(t-t_0)}, \tag{A20}$$

$$a_{k,\mathrm{vac}} \equiv -\frac{1}{\sqrt{2\pi}}\int_0^{+\infty} d\omega a_{k,0,\omega}(t_0)\, e^{-i\omega(t-t_0)}, \tag{A21}$$

$$b_{0,\mathrm{in}} \equiv -\frac{1}{\sqrt{2\pi}}\int_0^{+\infty} d\omega b_{0,\omega}(t_0)\, e^{i\omega(t_0-t)}, \tag{A22}$$

$$b_{i,\mathrm{in}} \equiv -\frac{1}{\sqrt{2\pi}}\int_0^{+\infty} d\omega b_{i,\omega}(t_0)\, e^{i\omega(t_0-t)}. \tag{A23}$$

Under the conditions $\kappa_{\mathrm{ex}} = \kappa_{R,\mathrm{ex}} = \kappa_{L,\mathrm{ex}}$, $\kappa_0 = \kappa_{R,0} = \kappa_{L,0}$, $\gamma_{\mathrm{in}} = \gamma_{1,\mathrm{in}} = \gamma_{2,\mathrm{in}}$, and $\gamma_0 = \gamma_{1,0} = \gamma_{2,0}$, we get the QLEs. (2)–(3) in the main text with $\kappa = \kappa_{\mathrm{ex}} + \kappa_0$ and $\gamma_m = \gamma_0 + \gamma_{\mathrm{in}}$.

APPENDIX B: THERMAL-NOISE SPECTRA BASED ON BRIGHT AND DARK MODES

In order to understand the thermal-noise cancellation around the frequency $\omega = \omega_m - J_m$, let us introduce the bright and dark modes $b_\pm$, i.e., the supermodes of the two coupled mechanical modes, as

$$b_\pm = \frac{1}{\sqrt{2}}\left(b_1 \pm b_2\right), \tag{B1}$$

then the Hamiltonian H_{sys} for optomechanical system under the rotating-wave approximation can be rewritten as

$$\begin{aligned} H_{\mathrm{sys}} = {} & \sum_{k=R,L}\left[\Delta_0 - g'\left(b_+^\dagger + b_+\right)\right]a_k^\dagger a_k \\ & + \sum_{k=R,L}\left[\Delta_0 - g'\left(b_-^\dagger + b_-\right)\right]a_k^\dagger a_k \\ & + \left(\omega_m + J_m\right)b_+^\dagger b_+ + \left(\omega_m - J_m\right)b_-^\dagger b_- \\ & + J_s\left(a_R^\dagger a_L + a_L^\dagger a_R\right) + \left(\Omega a_R^\dagger + \Omega^* a_R\right), \end{aligned} \tag{B2}$$

with $g' = g/\sqrt{2}$. Similarly, the free Hamiltonian of the optical and mechanical reservoirs H_{re} and the interaction Hamilton between the reservoirs and the optomechanical system H_{int} are rewritten as

$$\begin{aligned} H_{\mathrm{re}} = {} & \sum_{k=R,L}\int_0^{+\infty} d\omega\omega\left(a_{k,0,\omega}^\dagger a_{k,0,\omega} + a_{k,\mathrm{ex},\omega}^\dagger a_{k,\mathrm{ex},\omega}\right) \\ & + \int_0^{+\infty} d\omega\omega\left(B_{+,\omega}^\dagger B_{+,\omega} + B_{-,\omega}^\dagger B_{-,\omega} + b_{0,\omega}^\dagger b_{0,\omega}\right), \end{aligned} \tag{B3}$$

and

$$\begin{aligned} H_{\mathrm{int}} = {} & i\sum_{k=R,L}\int_0^{+\infty} d\omega h_{k,\mathrm{ex}}(\omega)\left[a_{k,\mathrm{ex},\omega}^\dagger a_k - a_k^\dagger a_{k,\mathrm{ex},\omega}\right] \\ & + i\sum_{k=R,L}\int_0^{+\infty} d\omega h_{k,0}(\omega)\left[a_{k,0,\omega}^\dagger a_k - a_k^\dagger a_{k,0,\omega}\right] \\ & + i\int_{-\infty}^{+\infty} d\omega g_{\mathrm{in}}(\omega)\left[B_{+,\omega}^\dagger b_+ - b_+^\dagger B_{+,\omega}\right] \\ & + i\int_{-\infty}^{+\infty} d\omega\sqrt{2}g_0(\omega)\left[b_{0,\omega}^\dagger b_+ - b_+^\dagger b_{0,\omega}\right] \\ & + i\int_{-\infty}^{+\infty} d\omega g_{\mathrm{in}}(\omega)\left[B_{-,\omega}^\dagger b_- - b_-^\dagger B_{-,\omega}\right], \end{aligned} \tag{B4}$$

where $B_{\pm,\omega} = \left(b_{1,\omega} \pm b_{2,\omega}\right)/\sqrt{2}$, $g_0(\omega) = g_{2,0}(\omega) = g_{1,0}(\omega)$, and $g_{\mathrm{in}}(\omega) = g_{1,\mathrm{in}}(\omega) = g_{2,\mathrm{in}}(\omega)$. The coupling strengths between the nanomechanical resonators and the reservoirs (R_0, R_1, and R_2) are summarized in Table I. We can see that the dark mode b_- with eigenvalue $\omega_m - J_m$ is decoupled from the common reservoir R_0, but the bright mode b_+ with eigenvalue $\omega_m + J_m$ is coupled to the common reservoir R_0 with the strength enhanced by a factor of $\sqrt{2}$. For this reason, the thermal noise for the dark mode b_-

TABLE I. Coupling strengths (CSs) between the nanomechanical resonators (NMRs) and the reservoirs (R_0, R_1, and R_2), for $g_0(\omega) = g_{2,0}(\omega) = g_{1,0}(\omega)$ and $g_{\rm in}(\omega) = g_{1,\rm in}(\omega) = g_{2,\rm in}(\omega)$.

Reservoirs	One NMR	Two NMRs			
	$b_1(\omega_m)$	$b_1(\omega_m)$	$b_2(\omega_m)$	$b_+(\omega_m + J_m)$	$b_-(\omega_m - J_m)$
CSs to R_0	g_0	g_0	g_0	$\sqrt{2}g_0$	0
CSs to R_1	$g_{\rm in}$	$g_{\rm in}$	0	$g_{\rm in}/\sqrt{2}$	$g_{\rm in}/\sqrt{2}$
CSs to R_2	0	0	$g_{\rm in}$	$g_{\rm in}/\sqrt{2}$	$g_{\rm in}/\sqrt{2}$

($\omega = \omega_m - J_m$) is suppressed dramatically, while thermal noise for the bright mode b_+ ($\omega = \omega_m + J_m$) is enhanced. Although the dark mode b_- is coupled to both the reservoirs R_1 and R_2, the coupling strengths are suppressed by a factor of $\sqrt{2}$. On the whole, the reservoir R_2 does not induce more thermal-noise effect.

Under the Markov approximation for $h_{k,\rm ex}(\omega) = \sqrt{\kappa_{k,\rm ex}/2\pi}$, $h_{k,0}(\omega) = \sqrt{\kappa_{k,0}/2\pi}$, $g_{\rm in}(\omega) = \sqrt{\gamma_{\rm in}/2\pi}$, and $g_0(\omega) = \sqrt{\gamma_0/2\pi}$, the dynamic equations for the operators a_k and $b_\pm$ are obtained as

$$\frac{da_R}{dt} = -i\left[\Delta_0 - g'\left(b_+^\dagger + b_+\right) - g'\left(b_-^\dagger + b_-\right)\right]a_R - iJ_s a_L - i\Omega - \frac{\kappa}{2}a_R + \sqrt{\kappa_{\rm ex}}a_{R,\rm in} + \sqrt{\kappa_0}a_{R,\rm vac}, \tag{B5}$$

$$\frac{da_L}{dt} = -i\left[\Delta_0 - g'\left(b_+^\dagger + b_+\right) - g'\left(b_-^\dagger + b_-\right)\right]a_L - iJ_s a_R - \frac{\kappa}{2}a_L + \sqrt{\kappa_{\rm ex}}a_{L,\rm in} + \sqrt{\kappa_0}a_{L,\rm vac}, \tag{B6}$$

$$\frac{db_+}{dt} = -\frac{\gamma_{\rm in} + 2\gamma_0}{2}b_+(t) - i(\omega_m + J_m)b_+ + ig'\left(a_R^\dagger a_R + a_L^\dagger a_L\right) + \sqrt{\gamma_{\rm in}}B_{+,\rm in} + \sqrt{2\gamma_0}b_{0,\rm in}, \tag{B7}$$

$$\frac{db_-}{dt} = -\frac{\gamma_{\rm in}}{2}b_-(t) - i(\omega_m - J_m)b_- + ig'\left(a_R^\dagger a_R + a_L^\dagger a_L\right) + \sqrt{\gamma_{\rm in}}B_{-,\rm in}, \tag{B8}$$

where $B_{\pm,\rm in}(t)$ is the input quantum noise defined by

$$B_{\pm,\rm in}(t) \equiv -\sqrt{\frac{1}{2\pi}}\int_0^{+\infty} d\omega B_{\pm,\omega}(t_0)\, e^{i\omega(t_0 - t)} \tag{B9}$$

with the correlation function

$$\left\langle B_{\pm,\rm in}^\dagger(\omega')\, B_{\pm,\rm in}(\omega)\right\rangle = N_{\rm th}\delta(\omega + \omega'). \tag{B10}$$

To calculate the spectra of the output fields, we linearize the nonlinear QLEs (B5)–(B8) by rewriting the operators as the sum of the mean values and the small quantum fluctuation terms as $a_k = \alpha_k + \delta a_k$ and $b_\pm = \beta_\pm + \delta b_\pm$. Keep only the first-order terms in the small quantum fluctuation terms δa_k and $\delta b_\pm$, the linearized QLEs read

$$\frac{d}{dt}\widetilde{V} = -\widetilde{M}\widetilde{V} + \widetilde{V}_{\rm in}, \tag{B11}$$

where we have the vector of the quantum fluctuation operators $\widetilde{V} = \left(\delta a_R\ \ \delta a_L\ \ \delta b_+\ \ \delta b_-\ \ \delta a_R^\dagger\ \ \delta a_L^\dagger\ \ \delta b_+^\dagger\ \ \delta b_-^\dagger\right)^T$, the vector of the input noise operators

$$\widetilde{V}_{\rm in} = \begin{pmatrix} \sqrt{\kappa_{\rm ex}}a_{R,\rm in} + \sqrt{\kappa_0}a_{R,\rm vac} \\ \sqrt{\kappa_{\rm ex}}a_{L,\rm in} + \sqrt{\kappa_0}a_{L,\rm vac} \\ \sqrt{\gamma_{\rm in}}B_{+,\rm in} + \sqrt{2\gamma_0}b_{0,\rm in} \\ \sqrt{\gamma_{\rm in}}B_{-,\rm in} \\ \sqrt{\kappa_{\rm ex}}a_{R,\rm in}^\dagger + \sqrt{\kappa_0}a_{R,\rm vac}^\dagger \\ \sqrt{\kappa_{\rm ex}}a_{L,\rm in}^\dagger + \sqrt{\kappa_0}a_{L,\rm vac}^\dagger \\ \sqrt{\gamma_{\rm in}}B_{+,\rm in}^\dagger + \sqrt{2\gamma_0}b_{0,\rm in}^\dagger \\ \sqrt{\gamma_{\rm in}}B_{-,\rm in}^\dagger \end{pmatrix}, \tag{B12}$$

and the matrix of the coefficients

$$\widetilde{M} = \begin{pmatrix} \frac{\kappa}{2} + i\omega_m & iJ_s & -iG_R' & -iG_R' & 0 & 0 & -iG_R' & -iG_R' \\ iJ_s & \frac{\kappa}{2} + i\omega_m & -iG_L' & -iG_L' & 0 & 0 & -iG_L' & -iG_L' \\ -iG_R'^* & -iG_L'^* & \frac{\gamma_+}{2} + i\omega_+ & 0 & -iG_R' & -iG_L' & 0 & 0 \\ -iG_R'^* & -iG_L'^* & 0 & \frac{\gamma_{\rm in}}{2} + i\omega_- & -iG_R' & -iG_L' & 0 & 0 \\ 0 & 0 & iG_R'^* & iG_R'^* & \frac{\kappa}{2} - i\omega_m & -iJ_s & iG_R'^* & iG_R'^* \\ 0 & 0 & iG_L'^* & iG_L'^* & -iJ_s & \frac{\kappa}{2} - i\omega_m & iG_L'^* & iG_L'^* \\ iG_R'^* & iG_L'^* & 0 & 0 & iG_R' & iG_L' & \frac{\gamma_+}{2} - i\omega_+ & 0 \\ iG_R'^* & iG_L'^* & 0 & 0 & iG_R' & iG_L' & 0 & \frac{\gamma_{\rm in}}{2} - i\omega_- \end{pmatrix} \tag{B13}$$

with $G_j' = g'\alpha_j$, $\gamma_+ = \gamma_{\rm in} + 2\gamma_0$, and $\omega_\pm = \omega_m \pm J_m$.

Based on the Fourier transform (20), the linearized QLEs (B11) can be solved in the frequency domain as

$$\widetilde{V}(\omega) = \widetilde{U}(\omega)\,\widetilde{V}_{\text{in}}(\omega), \tag{B14}$$

where $\widetilde{U}(\omega) = \left(\widetilde{M} - i\omega I\right)^{-1}$. The output spectra have the same form as Eqs. (25) and (26), where the transmission spectra are replaced by

$$T_R(\omega) = \left|\widetilde{U}_{11}(\omega)\,\kappa_{\text{ex}} - 1\right|^2 + \kappa_{\text{ex}}^2\left|\widetilde{U}_{15}(\omega)\right|^2, \tag{B15}$$

$$T_L(\omega) = \left|\kappa_{\text{ex}}\widetilde{U}_{22}(\omega) - 1\right|^2 + \kappa_{\text{ex}}^2\left|\widetilde{U}_{26}(\omega)\right|^2, \tag{B16}$$

the reflection spectra are replaced by

$$R_R(\omega) = \kappa_{\text{ex}}^2\left|\widetilde{U}_{12}(\omega)\right|^2 + \kappa_{\text{ex}}^2\left|\widetilde{U}_{16}(\omega)\right|^2, \tag{B17}$$

$$R_L(\omega) = \kappa_{\text{ex}}^2\left|\widetilde{U}_{21}(\omega)\right|^2 + \kappa_{\text{ex}}^2\left|\widetilde{U}_{25}(\omega)\right|^2, \tag{B18}$$

the thermal-noise spectra are replaced by

$$S_{R,\text{th}}(\omega) = S_{R,\text{th}}^{(+)}(\omega) + S_{R,\text{th}}^{(-)}(\omega), \tag{B19}$$

$$S_{L,\text{th}}(\omega) = S_{L,\text{th}}^{(+)}(\omega) + S_{L,\text{th}}^{(-)}(\omega), \tag{B20}$$

with

$$S_{R,\text{th}}^{(+)}(\omega) = \kappa_{\text{ex}}\gamma_+\left[\left|\widetilde{U}_{13}(\omega)\right|^2 + \left|\widetilde{U}_{17}(\omega)\right|^2\right]N_{\text{th}}, \tag{B21}$$

$$S_{R,\text{th}}^{(-)}(\omega) = \kappa_{\text{ex}}\gamma_{\text{in}}\left[\left|\widetilde{U}_{14}(\omega)\right|^2 + \left|\widetilde{U}_{18}(\omega)\right|^2\right]N_{\text{th}}, \tag{B22}$$

$$S_{L,\text{th}}^{(+)}(\omega) = \kappa_{\text{ex}}\gamma_+\left[\left|\widetilde{U}_{23}(\omega)\right|^2 + \left|\widetilde{U}_{27}(\omega)\right|^2\right]N_{\text{th}}, \tag{B23}$$

$$S_{L,\text{th}}^{(-)}(\omega) = \kappa_{\text{ex}}\gamma_{\text{in}}\left[\left|\widetilde{U}_{24}(\omega)\right|^2 + \left|\widetilde{U}_{28}(\omega)\right|^2\right]N_{\text{th}}, \tag{B24}$$

and the contribution from the incoming vacuum fields read

$$\begin{aligned} S_{R,\text{vac}}(\omega) = {} & \kappa_{\text{ex}}^2\left|\widetilde{U}_{15}(\omega)\right|^2 + \kappa_{\text{ex}}^2\left|\widetilde{U}_{16}(\omega)\right|^2 \\ & + \kappa_{\text{ex}}\kappa_0\left|\widetilde{U}_{15}(\omega)\right|^2 + \kappa_{\text{ex}}\kappa_0\left|\widetilde{U}_{16}(\omega)\right|^2 \\ & + \kappa_{\text{ex}}\gamma_+\left|\widetilde{U}_{17}(\omega)\right|^2 + \kappa_{\text{ex}}\gamma_{\text{in}}\left|\widetilde{U}_{18}(\omega)\right|^2, \end{aligned} \tag{B25}$$

$$\begin{aligned} S_{L,\text{vac}}(\omega) = {} & \kappa_{\text{ex}}^2\left|\widetilde{U}_{25}(\omega)\right|^2 + \kappa_{\text{ex}}\kappa_0\left|\widetilde{U}_{25}(\omega)\right|^2 \\ & + \kappa_{\text{ex}}^2\left|\widetilde{U}_{26}(\omega)\right|^2 + \kappa_{\text{ex}}\kappa_0\left|\widetilde{U}_{26}(\omega)\right|^2 \\ & + \kappa_{\text{ex}}\gamma_+\left|\widetilde{U}_{27}(\omega)\right|^2 + \kappa_{\text{ex}}\gamma_{\text{in}}\left|\widetilde{U}_{28}(\omega)\right|^2. \end{aligned} \tag{B26}$$

Here, $\widetilde{U}_{nm}(\omega)$ (for $n, m = 1, \ldots, 8$) denotes the element at the nth row and mth column of the matrix $\widetilde{U}(\omega)$.

[1] M. Aspelmeyer, T. J. Kippenberg, and F. Marquardt, Cavity optomechanics, Rev. Mod. Phys. **86**, 1391 (2014).

[2] H. Jing, S. K. Özdemir, X.-Y. Lü, J. Zhang, L. Yang, and F. Nori, $\mathcal{PT}$-Symmetric Phonon Laser, Phys. Rev. Lett. **113**, 053604 (2014).

[3] X.-W. Xu, Y.-x. Liu, C.-P. Sun, and Y. Li, Mechanical $\mathcal{PT}$ symmetry in coupled optomechanical systems, Phys. Rev. A **92**, 013852 (2015).

[4] Z.-P. Liu, J. Zhang, S. K. Özdemir, B. Peng, H. Jing, X.-Y. Lü, C.-W. Li, L. Yang, F. Nori, and Y.-x. Liu, Metrology with $\mathcal{PT}$-Symmetric Cavities: Enhanced Sensitivity Near the $\mathcal{PT}$-Phase Transition, Phys. Rev. Lett. **117**, 110802 (2016).

[5] J. Zhang, B. Peng, Ş. K. Özdemir, K. Pichler, D. O. Krimer, G. Zhao, F. Nori, Y.-x. Liu, S. Rotter, and L. Yang, A phonon laser operating at an exceptional point, Nat. Photon. **12**, 479 (2018).

[6] V. Peano, C. Brendel, M. Schmidt, and F. Marquardt, Topological Phases of Sound and Light, Phys. Rev. X **5**, 031011 (2015).

[7] L. Qi, Y. Xing, H.-F. Wang, A.-D. Zhu, and S. Zhang, Simulating Z_2 topological insulators via a one-dimensional cavity optomechanical cells array, Opt. Exp. **25**, 17948 (2017).

[8] M.-A. Lemonde, V. Peano, P. Rabl, and D. G. Angelakis, Quantum state transfer via acoustic edge states in a 2D optomechanical array, New J. Phys. **21**, 113030 (2019).

[9] X. Ni, S. Kim, and A. Alù, Topological insulator in two synthetic dimensions based on an optomechanical resonator, Optica **8**, 1024 (2021).

[10] H. Ren, T. Shah, H. Pfeifer, C. Brendel, V. Peano, F. Marquardt, and O. Painter, Topological phonon transport in an optomechanical system, Nat. Commun. **13**, 3476 (2022).

[11] J. Doster, T. Shah, T. Fösel, P. Paulitschke, F. Marquardt, and E. M. Weig, Observing polarization patterns in the collective motion of nanomechanical arrays, Nat. Commun. **13**, 2478 (2022).

[12] A. Youssefi, S. Kono, A. Bancora, M. Chegnizadeh, J. Pan, T. Vovk, and T. J. Kippenberg, Topological lattices realized in superconducting circuit optomechanics, Nature (London) **612**, 666 (2022).

[13] X.-W. Xu, Y.-J. Zhao, H. Wang, A.-X. Chen, and Y.-X. Liu, Generalized Su-Schrieffer-Heeger model in one dimensional optomechanical arrays, Front. Phys. **9**, 813801 (2022).

[14] S. Manipatruni, J. T. Robinson, and M. Lipson, Optical Nonreciprocity in Optomechanical Structures, Phys. Rev. Lett. **102**, 213903 (2009).

[15] M. Hafezi and P. Rabl, Optomechanically induced nonreciprocity in microring resonators, Opt. Exp. **20**, 7672 (2012).

[16] A. Metelmann and A. A. Clerk, Nonreciprocal Photon Transmission and Amplification via Reservoir Engineering, Phys. Rev. X **5**, 021025 (2015).

[17] X.-W. Xu and Y. Li, Optical nonreciprocity and optomechanical circulator in three-mode optomechanical systems, Phys. Rev. A **91**, 053854 (2015).

[18] B. Li, R. Huang, X. Xu, A. Miranowicz, and H. Jing, Nonreciprocal unconventional photon blockade in a spinning optomechanical system, Photon. Res. **7**, 630 (2019).

[19] X. Xu, Y. Zhao, H. Wang, H. Jing, and A. Chen, Quantum nonreciprocality in quadratic optomechanics, Photon. Res. **8**, 143 (2020).

[20] W. Nie, L. Wang, Y. Wu, A. Chen, and Y. Lan, Optomechanical ratchet resonators, Sci. China-Phys. Mech. Astron. **65**, 230311 (2022).
[21] G. S. Agarwal and S. Huang, Electromagnetically induced transparency in mechanical effects of light, Phys. Rev. A **81**, 041803 (2010).
[22] S. Weis, R. Rivière, S. Deléglise, E. Gavartin, O. Arcizet, A. Schliesser, and T. J. Kippenberg, Optomechanically induced transparency, Science **330**, 1520 (2010).
[23] A. H. Safavi-Naeini, T. P. M. Alegre, J. Chan, M. Eichenfield, M. Winger, Q. Lin, J. T. Hill, D. E. Chang, and O. Painter, Electromagnetically induced transparency and slow light with optomechanics, Nature (London) **472**, 69 (2011).
[24] F. Massel, T. T. Heikkilä, J. M. Pirkkalainen, S. U. Cho, H. Saloniemi, P. J. Hakonen, and M. A. Sillanpää, Microwave amplification with nanomechanical resonators, Nature (London) **480**, 351 (2011).
[25] F. Hocke, X. Zhou, A. Schliesser, T. J. Kippenberg, H. Huebl, and R. Gross, Electromechanically induced absorption in a circuit nano-electromechanical system, New J. Phys. **14**, 123037 (2012).
[26] Z. Shen, Y.-L. Zhang, Y. Chen, C.-L. Zou, Y.-F. Xiao, X.-B. Zou, F.-W. Sun, G.-C. Guo, and C.-H. Dong, Experimental realization of optomechanically induced non-reciprocity, Nat. Photon. **10**, 657 (2016).
[27] F. Ruesink, M.-A. Miri, A. Alù, and E. Verhagen, Nonreciprocity and magnetic-free isolation based on optomechanical interactions, Nat. Commun. **7**, 13662 (2016).
[28] Z. Shen, Y.-L. Zhang, Y. Chen, F.-W. Sun, X.-B. Zou, G.-C. Guo, C.-L. Zou, and C.-H. Dong, Reconfigurable optomechanical circulator and directional amplifier, Nat. Commun. **9**, 1797 (2018).
[29] F. Ruesink, J. P. Mathew, M.-A. Miri, A. Alù, and E. Verhagen, Optical circulation in a multimode optomechanical resonator, Nat. Commun. **9**, 1798 (2018).
[30] H. Qiu, J. Dong, L. Liu, and X. Zhang, Energy-efficient on-chip optical diode based on the optomechanical effect, Opt. Exp. **25**, 8975 (2017).
[31] X.-W. Xu, L. N. Song, Q. Zheng, Z. H. Wang, and Y. Li, Optomechanically induced nonreciprocity in a three-mode optomechanical system, Phys. Rev. A **98**, 063845 (2018).
[32] L. N. Song, Q. Zheng, X.-W. Xu, C. Jiang, and Y. Li, Optimal unidirectional amplification induced by optical gain in optomechanical systems, Phys. Rev. A **100**, 043835 (2019).
[33] J. Kim, M. C. Kuzyk, K. Han, H. Wang, and G. Bahl, Nonreciprocal Brillouin scattering induced transparency, Nat. Phys. **11**, 275 (2015).
[34] C.-H. Dong, Z. Shen, C.-L. Zou, Y.-L. Zhang, W. Fu, and G.-C. Guo, Brillouin-scattering-induced transparency and non-reciprocal light storage, Nat. Commun. **6**, 6193 (2015).
[35] M. Schmidt, S. Kessler, V. Peano, O. Painter, and F. Marquardt, Optomechanical creation of magnetic fields for photons on a lattice, Optica **2**, 635 (2015).
[36] K. Fang, J. Luo, A. Metelmann, M. H. Matheny, F. Marquardt, A. A. Clerk, and O. Painter, Generalized non-reciprocity in an optomechanical circuit via synthetic magnetism and reservoir engineering, Nat. Phys. **13**, 465 (2017).
[37] G. A. Peterson, F. Lecocq, K. Cicak, R. W. Simmonds, J. Aumentado, and J. D. Teufel, Demonstration of Efficient Nonreciprocity in a Microwave Optomechanical circuit, Phys. Rev. X **7**, 031001 (2017).
[38] N. R. Bernier, L. D. Tóth, A. Koottandavida, M. A. Ioannou, D. Malz, A. Nunnenkamp, A. K. Feofanov, and T. J. Kippenberg, Nonreciprocal reconfigurable microwave optomechanical circuit, Nat. Commun. **8**, 604 (2017).
[39] S. Barzanjeh, M. Wulf, M. Peruzzo, M. Kalaee, P. B. Dieterle, O. Painter, and J. M. Fink, Mechanical on-chip microwave circulator, Nat. Commun. **8**, 953 (2017).
[40] A. Metelmann and A. A. Clerk, Nonreciprocal quantum interactions and devices via autonomous feedforward, Phys. Rev. A **95**, 013837 (2017).
[41] L. Tian and Z. Li, Nonreciprocal quantum-state conversion between microwave and optical photons, Phys. Rev. A **96**, 013808 (2017).
[42] D. Malz, L. D. Tóth, N. R. Bernier, A. K. Feofanov, T. J. Kippenberg, and A. Nunnenkamp, Quantum-Limited Directional Amplifiers with Optomechanics, Phys. Rev. Lett. **120**, 023601 (2018).
[43] G. Li, X. Xiao, Y. Li, and X. Wang, Tunable optical nonreciprocity and a phonon-photon router in an optomechanical system with coupled mechanical and optical modes, Phys. Rev. A **97**, 023801 (2018).
[44] C. Jiang, L. N. Song, and Y. Li, Directional phase-sensitive amplifier between microwave and optical photons, Phys. Rev. A **99**, 023823 (2019).
[45] L. Mercier de Lépinay, E. Damskägg, C. F. Ockeloen-Korppi, and M. A. Sillanpää, Realization of Directional Amplification in a Microwave Optomechanical Device, Phys. Rev. Appl. **11**, 034027 (2019).
[46] Y. Chen, Y.-L. Zhang, Z. Shen, C.-L. Zou, G.-C. Guo, and C.-H. Dong, Synthetic Gauge Fields in a Single Optomechanical Resonator, Phys. Rev. Lett. **126**, 123603 (2021).
[47] X.-W. Xu, Y. Li, B. Li, H. Jing, and A.-X. Chen, Nonreciprocity via Nonlinearity and Synthetic Magnetism, Phys. Rev. Appl. **13**, 044070 (2020).
[48] Y.-B. Qian, D.-G. Lai, M.-R. Chen, and B.-P. Hou, Nonreciprocal photon transmission with quantum noise reduction via cross-Kerr nonlinearity, Phys. Rev. A **104**, 033705 (2021).
[49] A. Seif, W. DeGottardi, K. Esfarjani, and M. Hafezi, Thermal management and non-reciprocal control of phonon flow via optomechanics, Nat. Commun. **9**, 1207 (2018).
[50] S. Barzanjeh, M. Aquilina, and A. Xuereb, Manipulating the Flow of Thermal Noise in Quantum Devices, Phys. Rev. Lett. **120**, 060601 (2018).
[51] S. J. M. Habraken, K. Stannigel, M. D. Lukin, P. Zoller, and P. Rabl, Continuous mode cooling and phonon routers for phononic quantum networks, New J. Phys. **14**, 115004 (2012).
[52] H. Xu, L. Jiang, A. A. Clerk, and J. G. E. Harris, Nonreciprocal control and cooling of phonon modes in an optomechanical system, Nature (London) **568**, 65 (2019).
[53] D.-G. Lai, J.-Q. Liao, A. Miranowicz, and F. Nori, Noise-Tolerant Optomechanical Entanglement via Synthetic Magnetism, Phys. Rev. Lett. **129**, 063602 (2022).
[54] C. Sanavio, V. Peano, and A. Xuereb, Nonreciprocal topological phononics in optomechanical arrays, Phys. Rev. B **101**, 085108 (2020).
[55] I. Wilson-Rae, N. Nooshi, W. Zwerger, and T. J. Kippenberg, Theory of Ground State Cooling of a Mechanical

Oscillator Using Dynamical Backaction, Phys. Rev. Lett. **99**, 093901 (2007).
[56] F. Marquardt, J. P. Chen, A. A. Clerk, and S. M. Girvin, Quantum Theory of Cavity-Assisted Sideband Cooling of Mechanical Motion, Phys. Rev. Lett. **99**, 093902 (2007).
[57] L.-M. Duan and G.-C. Guo, Preserving Coherence in Quantum Computation by Pairing Quantum Bits, Phys. Rev. Lett. **79**, 1953 (1997).
[58] L. D. Contreras-Pulido and R. Aguado, Entanglement between charge qubits induced by a common dissipative environment, Phys. Rev. B **77**, 155420 (2008).
[59] Z. H. Wang, Y. J. Ji, Y. Li, and D. L. Zhou, Dissipation and decoherence induced by collective dephasing in a coupled-qubit system with a common bath, Phys. Rev. A **91**, 013838 (2015).
[60] S. Barzanjeh, A. Xuereb, S. Gröblacher, M. Paternostro, C. A. Regal, and E. M. Weig, Optomechanics for quantum technologies, Nat. Phys. **18**, 15 (2022).
[61] G. Anetsberger, O. Arcizet, Q. P. Unterreithmeier, R. Rivière, A. Schliesser, E. M. Weig, J. P. Kotthaus, and T. J. Kippenberg, Near-field cavity optomechanics with nanomechanical oscillators, Nat. Phys. **5**, 909 (2009).
[62] G. A. Brawley, M. R. Vanner, P. E. Larsen, S. Schmid, A. Boisen, and W. P. Bowen, Nonlinear optomechanical measurement of mechanical motion, Nat. Commun. **7**, 10988 (2016).
[63] H.-K. Li, Y.-C. Liu, X. Yi, C.-L. Zou, X.-X. Ren, and Y.-F. Xiao, Proposal for a near-field optomechanical system with enhanced linear and quadratic coupling, Phys. Rev. A **85**, 053832 (2012).
[64] M. Tsang and C. M. Caves, Coherent Quantum-Noise Cancellation for Optomechanical Sensors, Phys. Rev. Lett. **105**, 123601 (2010).
[65] J. Chan, T. P. M. Alegre, A. H. Safavi-Naeini, J. T. Hill, A. Krause, S. Gröblacher, M. Aspelmeyer, and O. Painter, Laser cooling of a nanomechanical oscillator into its quantum ground state, Nature (London) **478**, 89 (2011).
[66] G. S. MacCabe, H. Ren, J. Luo, J. D. Cohen, H. Zhou, A. Sipahigil, M. Mirhosseini, and O. Painter, Nano-acoustic resonator with ultralong phonon lifetime, Science **370**, 840 (2020).
[67] W. Yu, J. Wang, H. Y. Yuan, and J. Xiao, Prediction of Attractive Level Crossing via a Dissipative Mode, Phys. Rev. Lett. **123**, 227201 (2019).
[68] J. Zhao, Y. Liu, L. Wu, C.-K. Duan, Y.-x. Liu, and J. Du, Observation of Anti-$\mathcal{PT}$-Symmetry Phase Transition in the Magnon-Cavity-Magnon Coupled System, Phys. Rev. Appl. **13**, 014053 (2020).
[69] Y.-P. Wang and C.-M. Hu, Dissipative couplings in cavity magnonics, J. Appl. Phys. **127**, 130901 (2020).
[70] T. M. Karg, B. Gouraud, C. T. Ngai, G.-L. Schmid, K. Hammerer, and P. Treutlein, Light-mediated strong coupling between a mechanical oscillator and atomic spins 1 meter apart, Science **369**, 174 (2020).
[71] C. W. Gardiner and M. J. Collett, Input and output in damped quantum systems: Quantum stochastic differential equations and the master equation, Phys. Rev. A **31**, 3761 (1985).
[72] A. Bachtold, J. Moser, and M. I. Dykman, Mesoscopic physics of nanomechanical systems, Rev. Mod. Phys. **94**, 045005 (2022).
[73] X. Song, M. Oksanen, J. Li, P. J. Hakonen, and M. A. Sillanpää, Graphene Optomechanics Realized at Microwave Frequencies, Phys. Rev. Lett. **113**, 027404 (2014).
[74] P. Weber, J. Güttinger, A. Noury, J. Vergara-Cruz, and A. Bachtold, Force sensitivity of multilayer graphene optomechanical devices, Nat. Commun. **7**, 12496 (2016).
[75] V. Singh, S. J. Bosman, B. H. Schneider, Y. M. Blanter, A. Castellanos-Gomez, and G. A. Steele, Optomechanical coupling between a multilayer graphene mechanical resonator and a superconducting microwave cavity, Nat. Nanotechnol. **9**, 820 (2014).
[76] C. Dong, V. Fiore, M. C. Kuzyk, and H. Wang, Optomechanical dark mode, Science **338**, 1609 (2012).
[77] Y.-D. Wang and A. A. Clerk, Using Interference for High Fidelity Quantum State Transfer in Optomechanics, Phys. Rev. Lett. **108**, 153603 (2012).
[78] L. Tian, Adiabatic State Conversion and Pulse Transmission in Optomechanical Systems, Phys. Rev. Lett. **108**, 153604 (2012).
[79] D.-G. Lai, J.-F. Huang, X.-L. Yin, B.-P. Hou, W. Li, D. Vitali, F. Nori, and J.-Q. Liao, Nonreciprocal ground-state cooling of multiple mechanical resonators, Phys. Rev. A **102**, 011502 (2020).
[80] H.-M. Zhao, X.-J. Zhang, M. Artoni, G. C. La Rocca, and J.-H. Wu, Photon-pair generation on resonance via a dark state, Phys. Rev. A **106**, 023711 (2022).
[81] C. Doolin, B. D. Hauer, P. H. Kim, A. J. R. MacDonald, H. Ramp, and J. P. Davis, Nonlinear optomechanics in the stationary regime, Phys. Rev. A **89**, 053838 (2014).
[82] M. Asano, G. Zhang, T. Tawara, H. Yamaguchi, and H. Okamoto, Near-field cavity optomechanical coupling in a compound semiconductor nanowire, Commun. Phys. **3**, 230 (2020).
[83] I. S. Grudinin, H. Lee, O. Painter, and K. J. Vahala, Phonon Laser Action in a Tunable Two-Level System, Phys. Rev. Lett. **104**, 083901 (2010).
[84] H. Wang, Z. Wang, J. Zhang, S. K. Özdemir, L. Yang, and Y.-x. Liu, Phonon amplification in two coupled cavities containing one mechanical resonator, Phys. Rev. A **90**, 053814 (2014).
[85] S. Mahmoodian, P. Lodahl, and A. S. Sørensen, Quantum Networks with Chiral-Light–Matter Interaction in Waveguides, Phys. Rev. Lett. **117**, 240501 (2016).
[86] P. Lodahl, S. Mahmoodian, S. Stobbe, A. Rauschenbeutel, P. Schneeweiss, J. Volz, H. Pichler, and P. Zoller, Chiral quantum optics, Nature (London) **541**, 473 (2017).
[87] J. T. Hill, A. H. Safavi-Naeini, J. Chan, and O. Painter, Coherent optical wavelength conversion via cavity optomechanics, Nat. Commun. **3**, 1196 (2012).
[88] J. Bochmann, A. Vainsencher, D. D. Awschalom, and A. N. Cleland, Nanomechanical coupling between microwave and optical photons, Nat. Phys. **9**, 712 (2013).
[89] R. W. Andrews, R. W. Peterson, T. P. Purdy, K. Cicak, R. W. Simmonds, C. A. Regal, and K. W. Lehnert, Bidirectional and efficient conversion between microwave and optical light, Nat. Phys. **10**, 321 (2014).
[90] T. Bagci, A. Simonsen, S. Schmid, L. G. Villanueva, E. Zeuthen, J. Appel, J. M. Taylor, A. Sørensen, K. Usami, A. Schliesser, and E. S. Polzik, Optical detection of radio waves through a nanomechanical transducer, Nature (London) **507**, 81 (2014).

[91] C. Dong, V. Fiore, M. C. Kuzyk, L. Tian, and H. Wang, Optical wavelength conversion via optomechanical coupling in a silica resonator, Ann. Phys. **527**, 100 (2015).
[92] L. Tian, Optoelectromechanical transducer: Reversible conversion between microwave and optical photons, Ann. Phys. **527**, 1 (2015).
[93] M. Forsch, R. Stockill, A. Wallucks, I. Marinković, C. Gärtner, R. A. Norte, F. van Otten, A. Fiore, K. Srinivasan, and S. Gröblacher, Microwave-to-optics conversion using a mechanical oscillator in its quantum ground state, Nat. Phys. **16**, 69 (2020).
[94] Y.-W. Hu, Y.-F. Xiao, Y.-C. Liu, and Q. Gong, Optomechanical sensing with on-chip microcavities, Front. Phys. **8**, 475 (2013).
[95] M. Metcalfe, Applications of cavity optomechanics, Appl. Phys. Rev. **1**, 031105 (2014).
[96] B.-B. Li, L. Ou, Y. Lei, and Y.-C. Liu, Cavity optomechanical sensing, Nanophotonics **10**, 256 (2021).